Article

One-Pot Synthesis of Nitrogen-Doped TiO$_2$ with Supported Copper Nanocrystalline for Photocatalytic Environment Purification under Household White LED Lamp

Yixiao Pan [1], Yifei Wang [1], Shimiao Wu [1], Yating Chen [2], Xiangrong Zheng [2] and Ning Zhang [1,3,*]

[1] School of Materials Science and Engineering, Central South University, Changsha 410083, China; yixiaopan1@163.com (Y.P.); tjgjgt2@163.com (Y.W.); awsm2017@163.com (S.W.)

[2] Department of Pediatrics, Xiangya Hospital, Central South University, 87 Xiangya Road, Changsha 410008, China; yatingchen1111@163.com (Y.C.); xrzheng@csu.edu.cn (X.Z.)

[3] Guangdong Provincial Key Laboratory of Technique and Equipment for Macromolecular Advanced Manufacturing, South China University of Technology, Guangzhou 510640, China

* Correspondence: nzhang@csu.edu.cn

Abstract: Developing efficient and cheap photocatalysts that are sensitive to indoor light is promising for the practical application of photocatalysis technology. Here, N-doped TiO$_2$ photocatalyst with loaded Cu crystalline cocatalyst is synthesized by a simple one-pot method. The structure is confirmed by transmission electron microscopy and X-ray photoelectron spectroscopy analysis, which exhibit that Cu metal nanocrystalline is uniformly deposited on the surface of N-doped TiO$_2$ material. UV-Vis absorption spectra illustrate that the modified samples possess favorable visible light absorption properties and suppressed-electron hole separation. The as-fabricated Cu-loaded N-TiO$_2$ materials show high activity in photocatalytic decomposing isopropanol and inactivating *E. coli* under the irradiation of a household white LED lamp. The developed synthetic strategy and photocatalytic materials reported here are promising for indoor environment purification.

Keywords: photocatalysis; nitrogen-doped TiO$_2$; copper metal; isopropanol degradation; sterilization

1. Introduction

Photocatalysis is regarded as a promising approach for removing pollutants and harmful microbes [1–4]. To achieve the widespread practical application of photocatalytic environment remediation, efficient photocatalysts that are sensitive to weak visible light, especially indoor light, are required [5,6]. Among the various semiconductor photocatalysts, titanium dioxide (TiO$_2$) is one of the most promising materials for air purification and antibacterial functions due to its unique electronic band structures, prominent chemical stability, nontoxicity, and low cost [7,8]. However, TiO$_2$ is a typical wide bandgap semiconductor (~3.2 eV), and it is only activated by ultraviolet (UV) irradiation [9,10]. Doping TiO$_2$ with other elements is realized as an effective method to change the electronic band structure and, subsequently, the light absorption properties [11,12]. Over the past decades, the N-doped TiO$_2$, which possesses hybridization of N 2p and O 2p orbits with re-constructed valence band, shows decreased bandgap and visible light sensitivity [13,14]. Up to now, the N-doped TiO$_2$ is extensively studied as promising catalysts to decompose pollutants and microbes [15–17]; however, the activity is still unfavorable due to the easy recombination between photogenerated electrons and holes in bare materials [18,19]. To solve such a problem, loading cocatalysts such as Pt, Au, Ag, and other metals are effective in relieving the recombination of electron–hole pairs [20]. Especially, some non-noble metals such as Cu are more concerned as high activity and inexpensive cocatalyst materials to enhance the photocatalytic activity [21,22].

Up to now, the use of Cu metal cocatalysts to improve the photocatalytic activities over TiO$_2$ materials has been widely reported. For example, Wu et al. prepared Cu particles

deposited TiO_2 by 400 °C calcination/reduction under H_2 (3 mol% in N_2) atmosphere after incipient-wetness impregnation, and the photocatalytic activity for hydrogen evolution was significantly enhanced [23]. Chiang et al. synthesized Cu nanoparticles deposited TiO_2 nanorod composites by microwave-assisted sol–gel method and chemically reduced them with sodium borohydride as the reducing agent. The modified TiO_2 enhanced the photocatalytic degradation of bisphenol A [24]; however, previous fabrication of cocatalyst of Cu metal on TiO_2 is fabricated by mixture TiO_2 and Cu^{2+} based salt at high temperature in the presence of H_2. The TiO_2 can also be reduced into TiO_{2-x} and thus possibly decrease the intrinsic photocatalytic activity. The solvent reduction in the presence of sodium borohydride to reduce Cu^{2+} into Cu at mild conditions also seems effective; however, the process is sophisticated, and the reduced Cu metals usually have weak interaction with TiO_2, which is not beneficial to the photocatalytic process. Developing a facile method to fabricate Cu catalysts on TiO_2 with favorable photocatalytic activity is still limited.

In this study, the Cu-loaded on N-doped TiO_2 were synthesized by the one-pot reaction method. In such a fabrication process, the TiO_2 and Cu^{2+} salt simply mixed and then be nitridized in the presence of NH_3 at 775 K. The NH_3 at a high temperature can not only nitridize the TiO_2 into N-doped TiO_2, but also reduce the Cu^{2+} salt into Cu metal. The Cu metal loaded on N-TiO_2 could thus be achieved by the one-pot procedure. The interaction between catalyst and cocatalyst was difficult using such a synthetic process, which benefits the photocatalytic reactions. The UV-Vis absorption spectrum shows that fabricated materials exhibit favorable visible light absorption. The modified samples have a remarkable enhancement in remediating gaseous pollutants and microbes under indoor commercial LED irradiation. The developed one-pot synthetic strategy and Cu-loaded N-TiO_2 materials reported here are promising for the development of efficient photocatalysts for indoor environment purification.

2. Results and Discussion

The one-pot synthetic process is illustrated in Figure 1. Firstly, the $Cu(NO_3)_2$ and TiO_2 were mixed and ground; the $Cu(NO_3)_2$ thus adsorbed on the surface of TiO_2 nanoparticles. After that, the mixture was calcined under an ammonia atmosphere. The $Cu(NO_3)_2$ was reduced to Cu metal particles on the surface of TiO_2 in such a process: $NH_3 \rightarrow H_2 + N_2$ and $H_2 + Cu^{2+} \rightarrow Cu + 2H^+$. Meanwhile, a slight amount of N was doped into TiO_2 to generate N-doped TiO_2 (N-TiO_2). Finally, the Cu metal-supported N-doped TiO_2 was produced by the designed one-pot synthetic method. The products were expressed as xCu-N-TiO_2 (the x represented the weight ratio of loaded Cu to N-TiO_2).
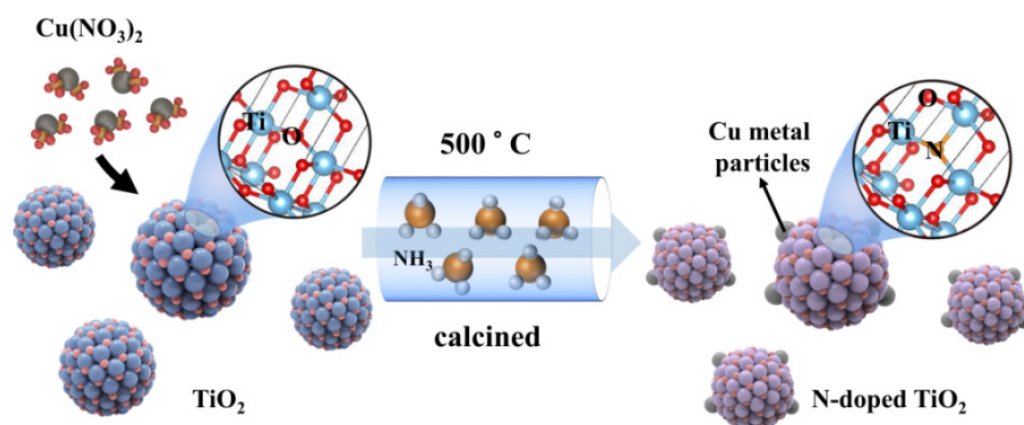

Figure 1. Scheme of synthesis of Cu metal loaded N-TiO_2 by one-pot process.

The X-ray diffraction (XRD) patterns of the pristine TiO_2, N-TiO_2, and xCu-N-TiO_2 samples are shown in Figure 2. All peaks of the as-prepared samples consist of anatase phases TiO_2 (JCPDS card. 21-1272) without other impurity peaks observed [25]. The half-peak width of all products is not changed significantly, indicating that the crystallinity

and grain size are almost kept. The copper and copper oxide are not observed, which is probably due to the fact that the amount of loaded Cu-based materials is too low to be detected by the XRD technical.
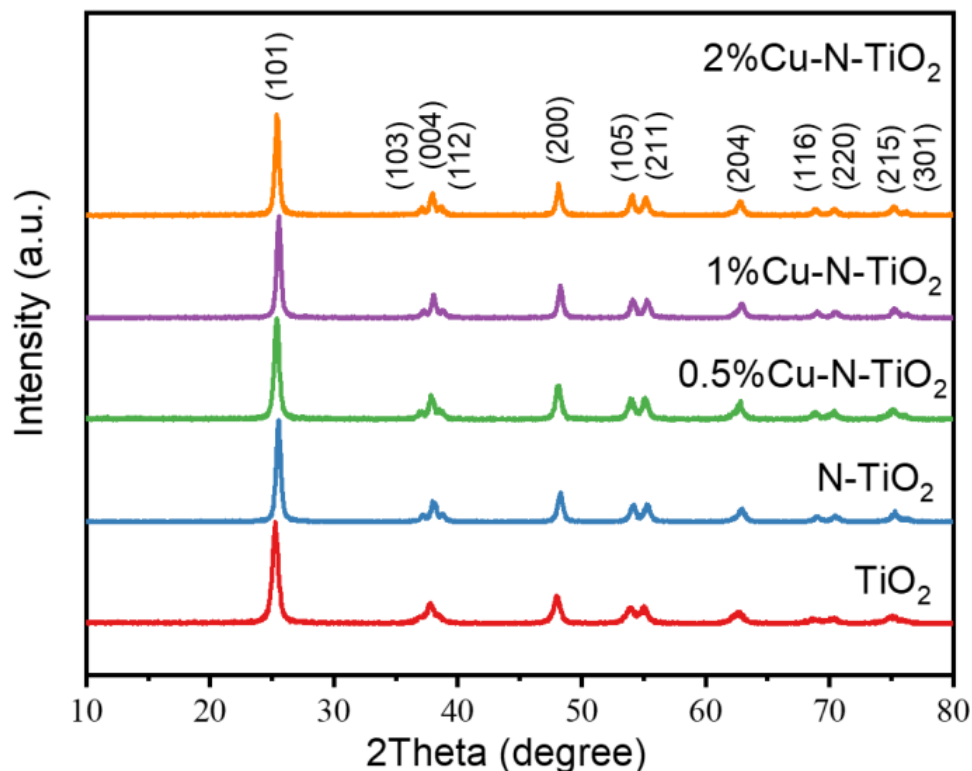

Figure 2. XRD pattern of TiO_2, $N-TiO_2$, and $xCu-N-TiO_2$ (x = 0.5%, 1%, and 2%).

Scanning electron microscopy (SEM) and transmission electron microscopy (TEM) were employed to characterize the morphologies and compositions of the as-prepared samples. Figure 3a and Figure S1 show the typical SEM images, which demonstrate that $1\%Cu-N-TiO_2$, $N-TiO_2$, and pristine TiO_2 photocatalysts have nanoparticle-like morphology where the size of these particles is about 20–50 nm. After nitridation and Cu loading, the size and morphology of the TiO_2 are not changed obviously. The TEM image in Figure 3b exhibits that materials of $1\%Cu-N-TiO_2$ are uniformly dispersed nanoparticles, which is identical to the SEM results. The selected area electronic diffraction (SAED) pattern displays well resolved (101), (004), and (205) diffraction rings (inset of Figure 3b), which corresponds to the structural characteristic of anatase TiO_2 [26]. The enlarged TEM image in Figure 3c further shows that the shape of each particle is an irregular shape with a narrow-distributed size from 20–50 nm. The high-resolution TEM (HRTEM) image of the product (Figure 3d) shows that the lattice fringe distance of the nanoparticles was measured as 0.35 and 0.36 nm, which corresponds to the (101) and (10$\bar{1}$) face of anatase TiO_2, respectively. In addition, some nanoparticles with a size of about 4 nm are loaded on the surface of TiO_2. As the HRTEM image illustrated, the lattice fringe is measured as 0.20 nm, which is consistent with the copper phase of Cu metal (111). Such a result indicates that the Cu metal nanoparticles are loaded on TiO_2 nanocrystals. To further confirm that the $Cu(NO_3)_2 \cdot 3H_2O$ can be converted into Cu metal under the designed synthetic condition, proper $Cu(NO_3)_2 \cdot 3H_2O$ powder was calcined in ammonia atmosphere under 500 °C without the addition of TiO_2. The XRD pattern in Figure S2 shows that all peaks were assigned to Cu metal. So, the Cu nanocrystalline loaded on N-doped TiO_2 nanoparticles is reasonable in our materials synthesis route.
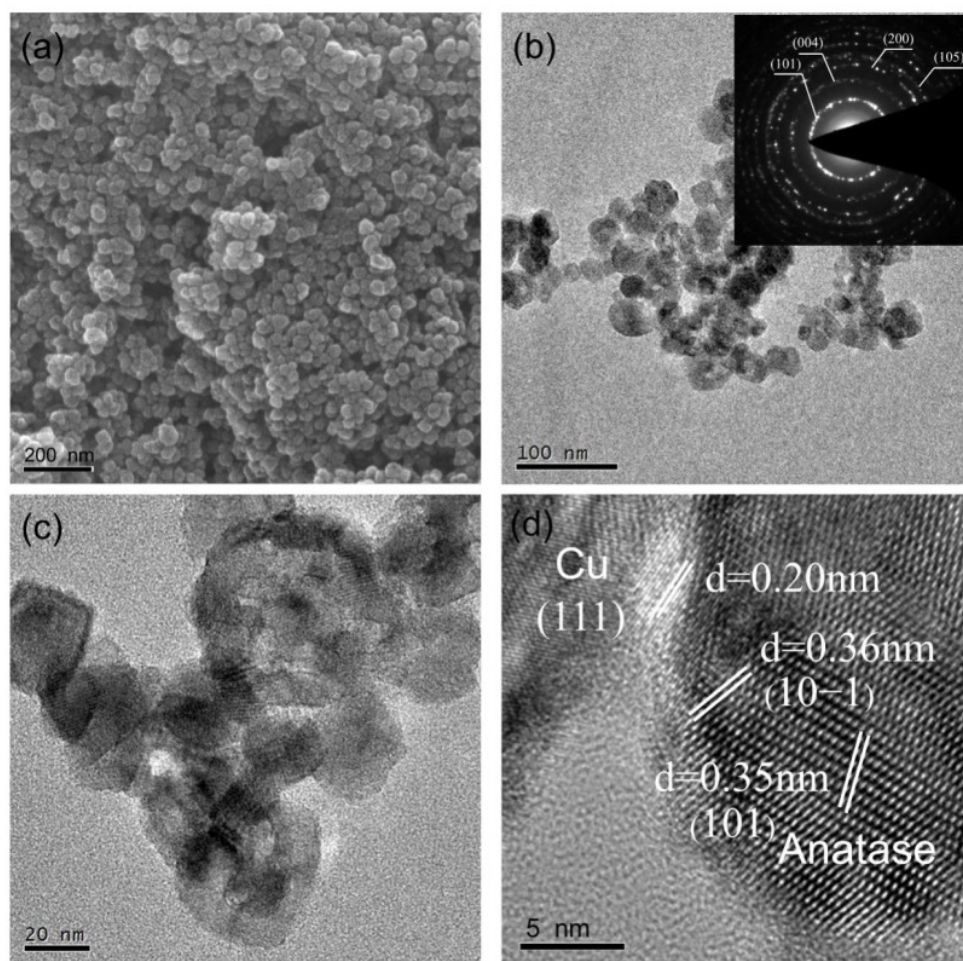
Figure 3. (**a**) SEM, (**b**–**d**) TEM, and SAED (inset) images of 1%Cu-N-TiO$_2$.

In the following study, the Cu states in 1%Cu-N-TiO$_2$ were determined through the Cu 2p XPS spectra. As shown in Figure 4a, the product of 1%Cu-N-TiO$_2$ displays one main peak located at 932.47 eV, which could be assigned to Cu^0 state [21]. Such a result suggests that the synthesized product is loaded with Cu metal. XPS element content analysis (Table S1) exhibits that the amount of loaded Cu is about 2 wt%, which is higher than the designed amount in our synthetic experiment. The variety in the amount of loaded may be because the XPS is a surface analysis technology, which detects the atoms on and near surface, which leads to the higher value of loaded Cu. The formed Cu metal nanoparticle on TiO$_2$ may partly be oxidized into the oxidation state of Cu$_2$O or CuO once it is exposed to air conditions; however, these characterizations show that the oxidation states of Cu, such as the CuO and Cu$_2$O, are not obvious. Figure 4b presents the XPS spectra of N1s state in N-TiO$_2$ and 1%Cu-N-TiO$_2$ samples. The binding energy range of N1s peaks is 396–404 eV, which is a typical N 1s XPS spectra for N-doped TiO$_2$ [27]. The binding energies of both samples are at 399.6 eV, which is considered as the form of Ti–N–O bonds [27,28]. So, the N element has been successfully doped into the TiO$_2$. Figure 4c and d present the XPS spectra of Ti 2p and O1s state in N-TiO$_2$ and 1%Cu-N-TiO$_2$ samples. The peak strength and peak position of the Ti 2p and O1s XPS spectra of the two samples were almost unchanged, indicating that Cu nanoparticles were only deposited on the surface of N-TiO$_2$ photocatalyst, which did not influence the chemical states of Ti and O.
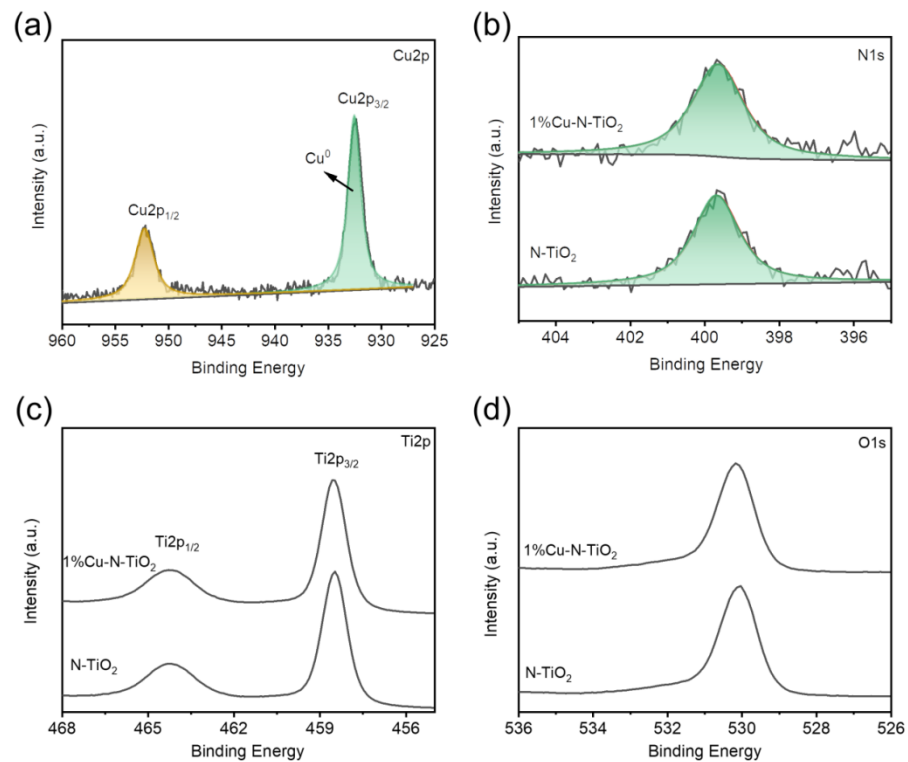
Figure 4. XPS spectra of: (**a**) Cu2p for 1%Cu-N-TiO$_2$ (**b**) N1s; (**c**) Ti2p; (**d**) O1s for N-TiO$_2$ and 1%Cu-N-TiO$_2$.

The UV-Vis absorption spectra of as-prepared materials were studied. Figure 5a shows that pristine TiO$_2$ have an absorption edge at about 380 nm. The N-doped TiO$_2$ products have much wider absorption edges. Figure 5b shows the enlarged areas from Figure 5a. It is observed that the N-TiO$_2$ and the Cu loaded can N-TiO$_2$ reach the absorption edge at about 540–560 nm. So, the light absorption ability is significantly enhanced. This can be attributed to the formation of a local intermediate band (N 2p) energy level at the top of the O 2p valence band in TiO$_2$ by the N introduction. The band gap of the semiconductor is narrowed so that longer wavelengths of light can be absorbed to form photogenerated electrons and holes [29,30]. It is worth noting that the loaded Cu metal particles have no obvious enhancement on the UV–Vis absorption spectra, which is attributed to the fact that the Cu element was only loaded on the surface of TiO$_2$, which did not change the electronic energy band structure of TiO$_2$.
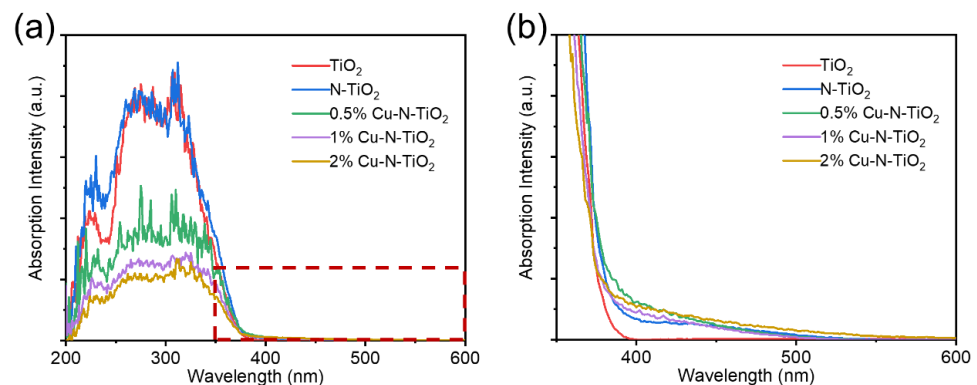

Figure 5. (**a**) UV-visible absorption spectrum and (**b**) the enlarged spectrum at 350–450 nm of pristine TiO$_2$, N- TiO$_2$, and xCu-N-TiO$_2$ nanocomposites (x = 0.5%, 1%, 2%).

The degradation of gaseous isopropanol (IPA) under white LED light irradiation is evaluated to reflect the photocatalytic performance of the prepared materials. IPA was chosen as the target molecule because it is a representative volatile organic compound for gaseous pollutants [31]. The wavelength of the indoor commercial white LED light used as a light source with a wavelength of 400–700 nm and light intensity of approximately 8 mW/cm^2 (Figure S3). Figure 6a shows a comparative study of the photocatalytic activity of acetone increases at full speed in the first 80 min over N-TiO$_2$ and different Cu loaded N-TiO$_2$ products. It could be found that the evolution rates of acetone over 2%Cu-N-TiO$_2$, 1%Cu-N-TiO$_2$, 0.5%Cu-N-TiO$_2$, and N-TiO$_2$ reach about 420.0, 662.3, 364.5, and 70.0 ppm h^{-1}, respectively. The 1%Cu-N-TiO$_2$ shows the best activity in the decomposing IPA, which is about 9.5 folds as N-TiO$_2$. Obviously, Cu nanoparticles on the surface of N-TiO$_2$ can act as cocatalysts and suppresses the recombination of the photogenerated hole–electron pairs, which improve the photocatalytic activity [32]. Figure 6b shows a complete process of IPA degradation under an LED light. Firstly, the concentration of IPA decrease fast with and the concentration of acetone increase rapidly (CH$_3$CHOHCH$_3$ + e$^-$ + O$_2$ + H$^+$ → CH$_3$COCH$_3$ + HO· + H$_2$O or CH$_3$CHOHCH$_3$ + h$^+$ → CH$_3$COCH$_3$+ 2H$^+$ + e$^-$) [33]. When the concentration of acetone reaches a maximum level, the concentration of acetone starts to be decomposed into CO$_2$, and the evolved CO$_2$ increases rapidly. Finally, the evolved concentration of CO$_2$ reaches about three times as initial concentration of IPA, indicating that 1%Cu-N-TiO$_2$ photocatalyst can mineralize IPA to CO$_2$ completely (CH$_3$CHOHCH$_3$ + 5H$_2$O + 18h$^+$ → 3CO$_2$ + 18H$^+$) [33,34].
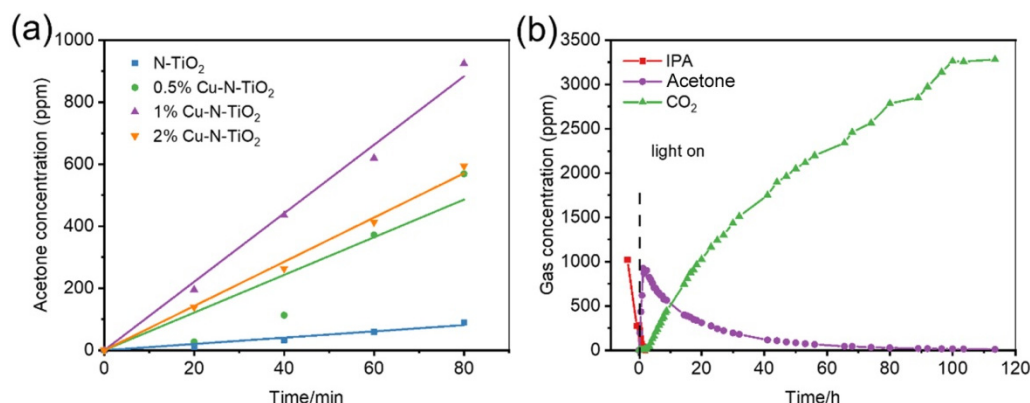

Figure 6. (**a**) Comparative studies of full speed acetone production over bare N-TiO$_2$, and xCu-N-TiO$_2$ (x = 0.5%, 1%, and 2%) samples under the same conditions; (**b**) representative time-dependent gas concentrations during IPA decomposition over 1%Cu-N-TiO$_2$ sample under LED light irradiation.

The Brunner−Emmet−Teller (BET) specific surface areas of the 1%Cu-N-TiO$_2$ and N-TiO$_2$ were determined using N$_2$ adsorption and desorption isotherms (Figure S4). The BET surface area of N-doped TiO$_2$ and 1%Cu-N-TiO$_2$ are approximate 29.7 and 31.9 m^{2}g^{-1}, which are quite closed. So, the degradation of activity is thus mainly influenced by the loading of Cu rather than the surface areas.

In the following study, the sterilization performance of 1%Cu-N-TiO$_2$ was evaluated under irradiation of indoor LED light. *E. coli* is one of the most common bacteria as a model microbe to evaluate the inactivation performance for many sterilization materials [35]. Figure 7a shows the corresponding activities of 1%Cu-N-TiO$_2$ and N-TiO$_2$. The survival rate of *E. coli* over 1%Cu-N-TiO$_2$ reaches 10^{-7} after 100 min, shows that the *E. coli* is completely sterilized. For comparison, the survival rate of *E. coli* over N-TiO$_2$ is only 0.33 in 100 min. So, the 1%Cu-N-TiO$_2$ shows much enhanced activity compared to N-TiO$_2$. In addition, the control experiments were carried out to prove that the sterilization effect is caused by the photocatalytic process over 1%Cu-N-TiO$_2$. When the 1%Cu-N-TiO$_2$ photocatalyst is placed in the bacterial culture medium under dark conditions, the bacteria surviving is closer to 100% after 120 min. So, there is no toxic effect of Cu-N-TiO$_2$ on *E. coli* cells under dark conditions. When the bacterial medium is placed under LED light

irradiation without catalyst, there is no obvious decrease in *E. coli* cells after 120 min. So, the activity is certain from the photocatalytic effects. Figure 7b,c show the images of *E. coli* colonies on agar plates before (diluted 10^5 times) and after (not diluted) LED light irradiation for 100 min in the presence of 1%Cu-N-TiO$_2$. During the photocatalytic process, the photogenerated electrons and holes pairs react with water to produce reactive oxygen species. The reactive oxygen species include HO$^\bullet$, O$_2^{\bullet-}$, HO$_2^\bullet$, etc., and can destroy the *E. coli* cell and results in bacterial inactivation [3].
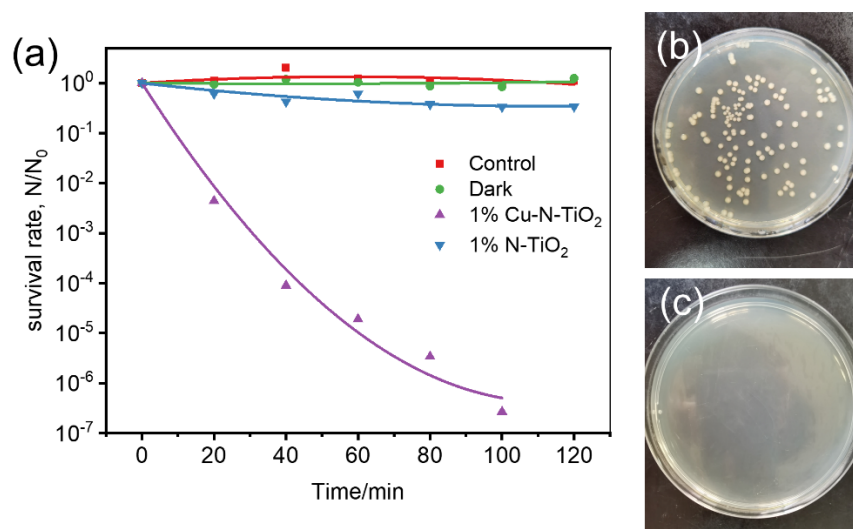
Figure 7. (**a**) Photocatalytic inactivation efficiency against *E. coli* (1×10^7 cfu mL^{-1}, 50 mL) in the presence of 1%Cu-N-TiO$_2$ and N-TiO$_2$ under LED light irradiation and control experiments; images of *E. coli* colonies on an agar plate (**b**) before (diluted 10^5 times) and (**c**) after (not diluted) LED light irradiation for 120 min in the presence of 1%Cu-N-TiO$_2$.

Figure 8 shows a scheme of as-prepared 1% Cu-N-TiO$_2$ for decomposition of IPA and inactivation of *E. coli*. Nitrogen doping forms an intermediate energy level on the top of the valence band in TiO$_2$ semiconductors, which shifts the absorption of light to the visible light region and induces the semiconductor to generate photogenerated electrons and holes under LED irradiation. The Cu metal nanoparticles act as a cocatalyst material on the surface of N-doped TiO$_2$ photocatalysts, which suppress the recombination of photogenerated electrons and holes. In addition, the metal state Cu can also act as electrons storage centers to promote multi-electron reactions. The photocatalytic decomposition of IPA and inactivation of *E. coli* efficiency is thus significantly improved under the irradiation of white LED light.
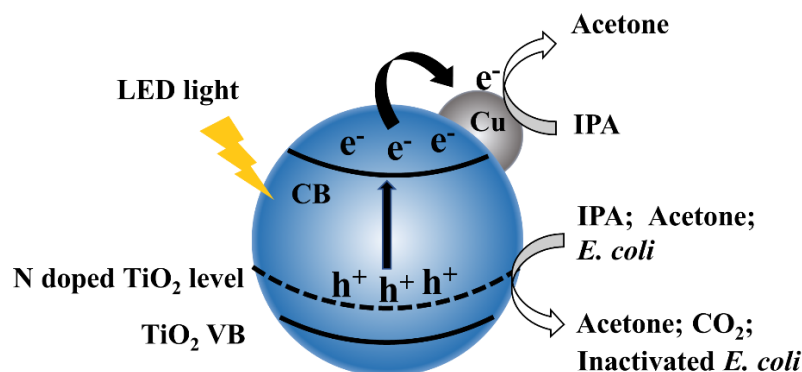

Figure 8. Schematic illustration of electronic bands structure and redox reactions over Cu loaded N-TiO$_2$ catalysts.

3. Materials and Methods

3.1. Preparation of Photocatalysts

In a typical process, 1.0 g TiO_2 (anatase phase, 10–25 nm grain size, Sigma-Aldrich Co. St. Louis, MO, USA) and $Cu(NO_3)_2 \cdot 3H_2O$ (AR, Sinopharm Chemical Reagent Co., Ltd., Shanghai, China) were well mixed with a certain ratio and ground. The mixture was calcined at 773 K for about 3 h under an ammonia atmosphere to obtain Cu metal-loaded N-doped TiO_2 nanoparticles (xCu-N-TiO_2). For comparison, pure TiO_2 powder was also calcined at 773 K in an ammonia atmosphere for 3 h without Cu, which was expressed as N-TiO_2.

3.2. Photocatalytic Degradation of Pollutants

The photocatalytic decomposition of gaseous isopropanol (IPA) was evaluated under white LED illumination. Figure S5 shows the reaction cell used in IPA degradation experiments. In a typical procedure, a 600 mL glass container was used as the photocatalytic vessel reactor. A commercial white LED (30 W, OPPLE, Shanghai, China) was located at 10 cm from the vessel reactor. About 100 mg photocatalysts were dispersed in a 9.5 cm^2 circular glass dish, which was located in the center of the vessel reactor. The reactor was filled with fresh synthetic air (20% oxygen and 80% nitrogen) for 1 h. The pressure inside the reactor was kept at 1 Kpa (Atmospheric pressure). Then, about 1000 ppm of gaseous IPA was injected into the reactor. The reactor was placed in darkness for 3 h to reach adsorption equilibrium. When the concentration of IPA remained constant, the adsorption equilibrium of IPA was considered to have been reached. During the process of IPA adsorption equilibrium, no products such as acetone or CO_2 were detected, indicating that the gaseous IPA could not be degraded by photocatalyst under dark conditions. The reactor was then irradiated with an LED lamp, and 0.5 mL products along the reactions were regularly extracted from the reactor. The concentrations of IPA, acetone, and CO_2 were measured by a gas chromatograph (GC-2014, Shimadzu, Kyoto, Japan).

3.3. Evaluation of Anti-Bacteria

The anti-bacteria activities of photocatalysts were evaluated by killing *E. coli* cells. The *E. coli* was cultured in Luria Bertani (LB) nutrient medium at 37 °C and shocked for 24 h. Then, the cultured *E. coli* cells were washed by centrifugation at 5000 rpm and were resuspended and diluted to ~1×10^7 cfu (colony forming unit)/mL in sterilized 0.9% saline solution. All glass apparatuses and consumables used in the experiments were sterilized in an autoclave at 121 °C for 25 min. About 30 mg photocatalyst was added to a glass reactor containing 30 mL diluted *E. coli* suspension. The reaction mixture was covered with quartz glass and stirred during the experiment. The light source was also produced from a commercial white LED (30 W, OPPLE) which was located 15 cm from the *E. coli* solution. The experimental temperature of photocatalysis was kept at about 25 °C by circulating cooling water. At regular intervals, an aliquot of the reaction solution was collected and diluted with saline solution, and 0.1 mL of the diluted solution was spread on a nutrient agar plate. The diluted *E. coli* cells were incubated at 37 °C for 24 h and then the number of viable cells was determined by counting colonies.

4. Conclusions

In summary, the Cu metal nanocrystalline-loaded N-TiO_2 photocatalysts were synthesized by a simple one-pot method. TEM, XPS, and UV-Vis absorption spectra confirm that Cu metal nanocrystalline is successfully deposited on N-doped TiO_2 photocatalysts and exhibits favorable visible light absorption ability. Under the irradiation of indoor white LED light, the IPA photodegradation rate over optimal 1%Cu-N-TiO_2 is about 662.3 ppm h^{-1}, which is about 9.5 folds as N-doped TiO_2 (70.0 ppm h^{-1}). The *E. coli* could be completely killed by 1%Cu-N-TiO_2 under LED light irradiation in 120 min, which is significantly improved in comparison with N-TiO_2. The developed synthetic strategy and photocatalytic

materials reported here are promising for the development of photocatalysts for indoor environment purification.

Supplementary Materials: Figure S1: SEM images of (a–c) pristine TiO_2, (d–f) N-TiO_2, and (g–h) 1%Cu-N-TiO_2. Figure S2: XRD pattern of product by nitridizing $Cu(NO_3)_2 \cdot 3H_2O$ powder under 773 K for about 3 h under NH_3 gas atmosphere. Figure S3: The irradiation spectrum of used white LED lamp. Figure S4: Nitrogen adsorption-desorption isotherms and calculated BET specific surface areas of the 1%Cu-N-TiO_2 and N-TiO_2. Figure S5: The reaction cell used for isopropanol degradation experiments. Table S1: XPS element content analysis of 1%Cu-N-TiO_2.

Author Contributions: Conceptualization, N.Z.; methodology, N.Z. and S.W.; software, Y.P.; validation, Y.P., Y.W. and Y.C.; formal analysis, Y.P.; investigation, Y.W.; resources, Y.P.; data curation, Y.P. and N.Z.; writing—original draft preparation, Y.P.; writing—review and editing, N.Z.; visualization, N.Z.; supervision, N.Z. and X.Z.; project administration, N.Z.; funding acquisition, N.Z. All authors have read and agreed to the published version of the manuscript.

Institutional Review Board Statement: Not applicable.

Informed Consent Statement: Not applicable.

Conflicts of Interest: The authors declare no conflict of interest.

Sample Availability: Samples of the compounds are available from the authors.

References

1. Gaya, U.I.; Abdullah, A.H. Heterogeneous photocatalytic degradation of organic contaminants over titanium dioxide: A review of fundamentals, progress and problems. *J. Photochem. Photobiol. C Photochem. Rev.* **2008**, *9*, 1–12. [CrossRef]
2. Vohra, A.; Goswami, D.Y.; Deshpande, D.A.; Block, S.S. Enhanced photocatalytic disinfection of indoor air. *Appl. Catal. B Environ.* **2006**, *64*, 57–65. [CrossRef]
3. Laxma Reddy, P.V.; Kavitha, B.; Kumar Reddy, P.A.; Kim, K.H. TiO_2-based photocatalytic disinfection of microbes in aqueous media: A review. *Environ. Res.* **2017**, *154*, 296–303. [CrossRef] [PubMed]
4. Baruah, S.; Dutta, J. Nanotechnology applications in pollution sensing and degradation in agriculture. *Environ. Chem. Lett.* **2009**, *7*, 191–204. [CrossRef]
5. Qiu, X.; Miyauchi, M.; Sunada, K.; Minoshima, M.; Liu, M.; Lu, Y.; Li, D.; Shimodaira, Y.; Hosogi, Y.; Kuroda, Y.; et al. Hybrid Cu_xO/TiO_2 Nanocomposites As Risk-Reduction Materials in Indoor. *ACS Nano* **2012**, *6*, 1609–1618. [CrossRef]
6. Pelaez, M.; Nolan, N.T.; Pillai, S.C.; Seery, M.K.; Falaras, P.; Kontos, A.G.; Dunlop, P.S.M.; Hamilton, J.W.J.; Byrne, J.A.; O'Shea, K.; et al. A review on the visible light active titanium dioxide photocatalysts for environmental applications. *Appl. Catal. B Environ.* **2012**, *125*, 331–349. [CrossRef]
7. Fujishima, A.; Zhang, X.; Tryk, D.A. TiO_2 photocatalysis and related surface phenomena. *Surf. Sci. Rep.* **2008**, *63*, 515–582. [CrossRef]
8. Hashimoto, K.; Irie, H.; Fujishima, A. TiO_2 photocatalysis: A historical overview and future prospects. *Jpn. J. Appl. Phys.* **2005**, *44*, 8269–8285. [CrossRef]
9. Ni, M.; Leung, M.K.H.; Leung, D.Y.C.; Sumathy, K. A review and recent developments in photocatalytic water-splitting using TiO2 for hydrogen production. Renew. *Sustain. Energy Rev.* **2007**, *11*, 401–425. [CrossRef]
10. Ohno, T.; Akiyoshi, M.; Umebayashi, T.; Asai, K.; Mitsui, T.; Matsumura, M. Preparation of S-doped TiO_2 photocatalysts and their photocatalytic activities under visible light. *Appl. Catal. A Gen.* **2004**, *265*, 115–121. [CrossRef]
11. Ren, W.; Ai, Z.; Jia, F.; Zhang, L.; Fan, X.; Zou, Z. Low temperature preparation and visible light photocatalytic activity of mesoporous carbon-doped crystalline TiO_2. *Appl. Catal. B Environ.* **2007**, *69*, 138–144. [CrossRef]
12. Basavarajappa, P.S.; Patil, S.B.; Ganganagappa, N.; Reddy, K.R.; Raghu, A.V.; Reddy, C.V. Recent progress in metal-doped TiO_2, non-metal doped/codoped TiO_2 and TiO_2 nanostructured hybrids for enhanced photocatalysis. *Int. J. Hydrogen Energy* **2020**, *45*, 7764–7778. [CrossRef]
13. Asahi, R.; Morikawa, T.; Ohwaki, T.; Aoki, K.; Taga, Y. Visible-light photocatalysis in nitrogen-doped titanium oxides. *Science* **2001**, *293*, 269–271. [CrossRef]
14. Rengifo-Herrera, J.A.; Mielczarski, E.; Mielczarski, J.; Castillo, N.C.; Kiwi, J.; Pulgarin, C. Escherichia coli inactivation by N, S co-doped commercial TiO2 powders under UV and visible light. *Appl. Catal. B Environ.* **2008**, *84*, 448–456. [CrossRef]

15. Chen, X.; Xie, Z.; Liang, Y.; Wei, J.; Zhu, Y.; Huo, Y.; Zhang, X.; Wang, H. Hybridizing TiO_2 with Nitrogen-Doped Carbon: A New Route to A Highly Visible Light-Active Photocatalyst. *ChemistrySelect* **2017**, *2*, 1565–1572. [CrossRef]

16. Li, G.; Zou, B.; Feng, S.; Shi, H.; Liao, K.; Wang, Y.; Wang, W.; Zhang, G. Synthesis of N-Doped TiO_2 with good photocatalytic property. *Phys. B Condens. Matter* **2020**, *588*, 412184. [CrossRef]

17. Dunnill, C.W.; Parkin, I.P. Nitrogen-doped TiO_2 thin films: Photocatalytic applications for healthcare environments. *Dalton Trans.* **2011**, *40*, 1635–1640. [CrossRef] [PubMed]

18. Kumar, S.G.; Devi, L.G. Review on modified TiO_2 photocatalysis under UV/visible light: Selected results and related mechanisms on interfacial charge carrier transfer dynamics. *J. Phys. Chem. A* **2011**, *115*, 13211–13241. [CrossRef]

19. Low, J.; Yu, J.; Jaroniec, M.; Wageh, S.; Al-Ghamdi, A.A. Heterojunction Photocatalysts. *Adv. Mater.* **2017**, *29*. [CrossRef] [PubMed]

20. Tada, H.; Kiyonaga, T.; Naya, S.I. Rational design and applications of highly efficient reaction systems photocatalyzed by noble metal nanoparticle-loaded titanium(IV) dioxide. *Chem. Soc. Rev.* **2009**, *38*, 1849–1858. [CrossRef]

21. Zhai, S.; Yang, X.; Tang, M.; Gu, W.; Teng, F. Facile Synthesis of Cu Quantum Dots-TiO_2 Nanosheets Schottky Junction and Improved Photocatalytic Degradation Activity. *ChemistrySelect* **2020**, *5*, 5693–5700. [CrossRef]

22. Hao, W.; Zhao, L.; Li, X.; Qin, L.; Han, S.; Kang, S.Z. Cu nanoclusters incorporated mesoporous TiO2 nanoparticles: An efficient and stable noble metal-free photocatalyst for light driven H2 generation. *Int. J. Hydrogen Energy* **2021**, *46*, 6461–6473. [CrossRef]

23. Wu, N.L.; Lee, M.S. Enhanced TiO_2 photocatalysis by Cu in hydrogen production from aqueous methanol solution. *Int. J. Hydrogen Energy* **2004**, *29*, 1601–1605. [CrossRef]

24. Chiang, L.F.; Doong, R. An Cu-TiO_2 nanorods with enhanced ultraviolet- and visible-light photoactivity for bisphenol A degradation. *J. Hazard. Mater.* **2014**, *277*, 84–92. [CrossRef] [PubMed]

25. Gu, L.; Wang, J.; Cheng, H.; Du, Y.; Han, X. Synthesis of nano-sized anatase TiO_2 with reactive (001) facets using lamellar protonated titanate as precursor. *Chem. Commun.* **2012**, *48*, 6978–6980. [CrossRef] [PubMed]

26. Miao, L.; Tanemura, S.; Toh, S.; Kaneko, K.; Tanemura, M. Heating-sol-gel template process for the growth of TiO_2 nanorods with rutile and anatase structure. *Appl. Surf. Sci.* **2004**, *238*, 175–179. [CrossRef]

27. Xu, T.; Wang, M.; Wang, T. Effects of N Doping on the Microstructures and Optical Properties of TiO_2. *J. Wuhan Univ. Technol.-Mater. Sci. Ed.* **2019**, *34*, 55–63. [CrossRef]

28. Yang, G.; Jiang, Z.; Shi, H.; Xiao, T.; Yan, Z. Preparation of highly visible-light active N-doped TiO_2 photocatalyst. *J. Mater. Chem.* **2010**, *20*, 5301–5309. [CrossRef]

29. Di Valentin, C.; Pacchioni, G.; Selloni, A.; Livraghi, S.; Giamello, E. Characterization of paramagnetic species in N-doped TiO_2 powders by EPR spectroscopy and DFT calculations. *J. Phys. Chem. B* **2005**, *109*, 11414–11419. [CrossRef]

30. Di Valentin, C.; Pacchioni, G.; Selloni, A. Origin of the different photoactivity of N-doped anatase and rutile TiO_2. *Phys. Rev. B-Condens. Matter Mater. Phys.* **2004**, *70*, 1–4. [CrossRef]

31. Wolkoff, P.; Nielsen, G.D. Organic compounds in indoor air-their relevance for perceived indoor air quality? *Atmos. Environ.* **2001**, *35*, 4407–4417. [CrossRef]

32. Ombaka, L.M.; Curti, M.; McGettrick, J.D.; Davies, M.L.; Bahnemann, D.W. Nitrogen/Carbon-Coated Zero-Valent Copper as Highly Efficient Co-catalysts for TiO_2 Applied in Photocatalytic and Photoelectrocatalytic Hydrogen Production. *ACS Appl. Mater. Interfaces* **2020**, *12*, 30365–30380. [CrossRef] [PubMed]

33. Ouyang, S.; Ye, J. β-AgAl1-xGaxO$_2$ solid-solution photocatalysts: Continuous modulation of electronic structure toward high-performance visible-light photoactivity. *J. Am. Chem. Soc.* **2011**, *133*, 7757–7763. [CrossRef] [PubMed]

34. Arsac, F.; Bianchi, D.; Chovelon, J.M.; Ferronato, C.; Herrmann, J.M. Experimental microkinetic approach of the photocatalytic oxidation of isopropyl alcohol on TiO_2. Part 1. Surface elementary steps involving gaseous and adsorbed C_3HxO species. *J. Phys. Chem. A* **2006**, *110*, 4202–4212. [CrossRef] [PubMed]

35. Venieri, D.; Fraggedaki, A.; Kostadima, M.; Chatzisymeon, E.; Binas, V.; Zachopoulos, A.; Kiriakidis, G.; Mantzavinos, D. Solar light and metal-doped TiO_2 to eliminate water-transmitted bacterial pathogens: Photocatalyst characterization and disinfection performance. *Appl. Catal. B Environ.* **2014**, *154–155*, 93–101. [CrossRef]